Plant trait heterosis is quantitatively associated with expression heterosis of the plastid ribosomal proteins

Devon Birdseye[1], Laura A. de Boer[1], Hua Bai[1], Peng Zhou[2], Zhouxin Shen[1], Eric A. Schmelz[1], Nathan M. Springer[2], Steven P. Briggs[1]

[1] Division of Biological Sciences, University of California, San Diego, La Jolla, CA 92093, USA

[2] Department of Plant and Microbial Biology, University of Minnesota, Saint Paul, MN 55108, USA

Abstract

The use of hybrids is widespread in agriculture, yet the molecular basis for hybrid vigor (heterosis) remains obscure. To identify molecular components that may contribute to the known higher photosynthetic capacity of maize hybrids, we generated paired datasets of the proteomes and transcriptomes from leaf tissues of maize hybrids and their inbred parents. Expression patterns in the hybrids were semi-dominant to overdominant for subunits of the digenomic protein complexes required for the light reactions of photosynthesis and for chloroplast protein synthesis; nuclear and plastid-encoded subunits were elevated similarly. These patterns were not mirrored in the nuclear transcriptomes. We compared growth to transcript and protein levels of multiple hybrids with varying levels of heterosis. Expression heterosis (hybrid/mid-parent expression levels) of chloroplast ribosomal proteins and of nuclear transcripts for the photosynthetic light reactions was positively correlated with plant height heterosis (hybrid/mid-parent plant height). Ethylene biosynthetic enzymes were expressed below mid-parent levels in the hybrids, and the ethylene biosynthesis mutant *acs2/acs6* partially phenocopied the hybrid proteome, indicating that a reduction in ethylene biosynthesis may be upstream of the elevated expression of photosynthetic and ribosomal proteins in chloroplasts of hybrids.

Introduction

Plants, animals, and humans display inbreeding depression associated with increased genetic uniformity and characterized by reduced vigor (Schnable & Springer, 2013b). Mating between genetically distinct inbred parents can produce hybrid progeny that display dramatically

increased vigor, with many traits outperforming both parents. Heterosis is typically defined as the difference in vigor between a hybrid and (a) the average of its parents or (b) the better-performing parent. Heterosis can provide a major increase in fitness. Sexually compatible but genetically distinct species that mate in the wild can give rise to natural hybrids that out-compete their parents in the same niche (Rosenfield et al., 2004). Hybrids may out-perform their parents in terms of size, vigor, yield, abiotic and biotic stress resistance, and reproductive advantage (Dobzhansky, 1950; Shull, 1948). The magnitude of increased vigor caused by hybridity can be so great that crop and livestock species have been bred as hybrids for decades, despite the greater time and cost required for a hybrid breeding program (Troyer, 2006).

Neither heterosis nor inbreeding depression are fully understood. QTL mapping has shown that minor effect loci for heterosis are distributed throughout the genome (Schnable & Springer, 2013a). Transcriptome (Stupar et al., 2008) and proteome (Hu et al., 2017a) profiles indicate that gene expression levels in hybrids are generally the average of their parents, whereas traits of a hybrid can be much greater than either parent. A minority of mRNAs and proteins are expressed above or below mid-parent (MP) levels and most of these gene products are not obviously related to each other in function or to hybrid phenotypes, making their unusual levels difficult to interpret (Zhou et al., 2013). Despite these ambiguities, progress has been made in understanding hybrid vigor.

Recent work has implicated the plant hormone ethylene (ET) in heterosis. Maize hybrids display a temporal shift in circadian-mediated gene expression, causing down-regulation of ET biosynthesis genes (Ko et al., 2016). Knock-down of ET biosynthesis in maize hybrids enhanced their agronomic performance (Habben et al., 2014). In Arabidopsis hybrids, ET is produced at reduced levels and application of exogenous ET reduced hybrid vigor (Q. Song et al., 2018). Thus, ET potentially mediates at least some aspects of heterosis.

Previous work has reported elevated expression of eukaryotic ribosomal proteins in roots of the maize hybrid, Mo17xB73 (Marcon et al., 2013). Of 17 non-additively expressed ribosomal proteins, 16 displayed high or above high parent expression, also referred to as dominant and over-dominant expression. The authors speculate that a higher protein synthesis rate might

promote hybrid vigor. Subsequent proteomic studies in both maize and Arabidopsis reported similar observations of increased expression of proteins related to translation in hybrids (Dahal et al., 2016; Guo et al., 2013; Hu et al., 2017b; Rockenbach et al., 2018).

Maize hybrids have greater photosynthetic capacity than their inbred parents (Ko et al., 2016). In both maize and Arabidopsis, various genes for photosynthesis have been reported to be expressed above mid-parent levels (Fujimoto et al., 2012; Ko et al., 2016; Y. Song et al., 2016). An analysis of enzyme and metabolite levels in maize hybrids showed that metabolites and enzymes of the photosynthetic carbon reactions are elevated in hybrids whereas metabolites and enzymes of the photorespiratory pathway are reduced (Li et al., 2020). The authors hypothesize that reduced levels of toxic metabolites generated by photorespiration may contribute substantially to heterosis.

We reasoned that combined proteome and transcriptome profiles would be more likely than either alone to reveal differences that have physiological consequences. Transcript and protein networks made from the same tissue samples show relatively little overlap indicating a natural complementarity arising from post-transcriptional regulation (Walley et al., 2013, 2016). Transcript profiles generally include more genes than proteome profiles although only the proteome includes the products expressed from organelle genomes. Paired data sets were created using RNA-seq and peptide mass spectrometry on the same tissue samples to examine juvenile leaves and mature leaf blades of hybrids for molecular phenotypes including non-additive expression levels in hybrids. These expression values were calculated by dividing the hybrid expression level by the mid-parent level (mid-parent, or MP, is the average expression level of the parents) or by the high-parent level (HP). We found mostly overdominant expression of digenomic protein complexes in plastids. Digenomic complexes contain subunits from both the nuclear and plastid genomes. They mostly function in the light reactions of photosynthesis and in translation of plastid mRNAs. In contrast, most plastid-localized proteins are nuclear-encoded and were expressed at mid-parent levels.

Additionally, we analyzed the transcriptome and proteome across a range of hybrids with varying levels of growth heterosis to identify expression patterns that correlated with vigor. We

found that expression heterosis levels of plastid ribosomal proteins were positively correlated with growth heterosis; this correlation was weaker for their transcripts. Conversely, transcript levels for subunits of the light reaction complexes were positively correlated with growth heterosis; this correlation was weaker for their proteins. The elevated expression of digenomic protein complexes was phenocopied in the ET biosynthesis mutant, *acs2-6*, indicating that reduced ET levels play key roles in the molecular phenotypes of maize hybrids.

Results

Overdominant Expression of Photosynthetic Complexes

Genome-wide expression measurements based on ratios of isotope-coded peptide tags for proteins and on RNA-seq for transcripts provided high reproducibility between biological replicates (Supplemental Figure S1). The same frozen leaf tissue was extracted and used for generating mRNA and protein data to facilitate comparisons between the transcriptome and proteome. Protein expression levels in seedling and mature leaf blades of the hybrid, B73xMo17, were compared to the calculated MP levels of the inbred parents in four independent experiments (Figure 1; Supplemental Data Set 1). Total leaf proteome levels in the hybrid were additive and centered on their MP values, and levels in the inbreds were similar to each other (grey circles). While most plastid-localized proteins were not consistently expressed outside mid-parental range, most plastid genome-encoded proteins were selectively expressed 10-20% above their MP levels. Many are subunits of energy-transducing complexes located in the thylakoid membranes and are encoded by Photosynthesis Associated Plastid Genes (PhAPGs). Additional subunits of these complexes are encoded by Photosynthesis Associated Nuclear Genes (PhANGs); these nuclear counterparts were similarly selectively expressed above MP levels. The PhAPG/PhANG proteins comprise photosystem I, photosystem II, the cytochrome b6/f complex, NAD(P)H dehydrogenase-like complex, and ATP synthase. This pattern included the carbon-fixation enzyme, Rubisco, which also is comprised of subunits from the nuclear and plastid genomes. Readers can use our website to visualize expression of their chosen genes in the hybrid compared to mid-parent levels (https://devonbirdseye.shinyapps.io/ExpressionViewer/).

Expression of the plastid ribosomal proteins seemed to be more responsive to circumstances; they were above mid-parent levels in three experiments and below in one. The circumstances

that caused the observed variations were not identified. One possible influence is light intensity, which is known to increase heterosis in *Antirrhinum* (Haney WJ, Gartner JB, 1953) and Arabidopsis (Meyer et al., 2004); we did not control for light intensity in our experiments.

Proteins that were expressed above MP levels were also frequently expressed at different levels between the parents, and expression in B73 was higher than in Mo17 in most cases. Exceptions included photosynthetic electron transfer C, ribose-5-phosphate isomerase, and the oxygen evolving complex assembly proteins; these were expressed higher in Mo17, providing opportunities for biochemical complementation in the hybrid (Supplemental Data Set 1). Comparison of protein expression in hybrids relative to the high-parent levels revealed an overdominant expression pattern for the PhANGs/PhAPGs, and a mostly dominant pattern for the plastid ribosomal proteins (Figure S2).

The proteome differences between plastids of the hybrid and its inbred parents were not mirrored in their nuclear transcriptomes (Figure S3). The nuclear transcripts for PhANGs were slightly elevated in the hybrid seedling leaf, less than their corresponding proteins. However, PhANG transcript expression levels were not elevated in the hybrid leaf blade, discordant with their proteins. Expression heterosis levels of nuclear transcripts for plastid ribosomal proteins varied between experiments and were discordant to their protein abundance. In the seedling leaf, their expression was consistently higher in Mo17 than B73, while their protein expression was higher in B73 than Mo17. These results imply that post-transcriptional regulation of plastid ribosomal protein levels and PhANG protein levels is substantial. Plastid-encoded transcripts were not measured.

To determine whether the results observed with B73xMo17 are similar in other maize hybrids we examined a set of six hybrids that included a new tissue sample from the previously characterized, B73xMo17. Both B73xMo17 and its reciprocal hybrid, Mo17xB73 (Mo17 is the female parent), displayed the same molecular phenotypes as described above, indicating that the differences are not due to maternal or cytoplasmic effects (Figure S4 A-B). Inbreds B73 and B84 are members of the Stiff Stalk pool of germplasm whereas inbreds Mo17 and A682 are part of the Lancaster pool. Hybrids made from crosses between these pools have strong heterosis.

Hybrids made from crosses within each pool have reduced heterosis (Dudley et al., 1991). We found that every hybrid expressed PhAPG and PhANG proteins above MP levels, whether or not there was strong heterosis (Figure S4 C-F). In contrast, the plastid ribosomal proteins were expressed at or below MP levels in the hybrids with low levels of heterosis and substantially above MP levels in the hybrids with high levels of heterosis. Thus, the PhAPG and PhANG protein expression was above mid-parent levels with both high and low levels of heterozygosity/heterosis whereas the plastid ribosomal protein levels responded proportionately to the degree of heterozygosity/heterosis. The PhAPG and PhANG proteins and plastid ribosomal proteins were expressed higher in the Stiff Stalk inbreds (B73, B84) than in the Lancaster inbreds (Mo17, A682). The levels in Stiff Stalk inbreds were similar to each other; likewise for the Lancaster inbreds. As noted previously for the plastid ribosome, the pattern of differential expression between inbreds was discordant between transcripts and proteins (Figure S5).

Expression heterosis is consistent between the seedling leaf and the mature leaf blade (Figure S6 A and B). Differences in expression between B73 and Mo17 also remain consistent between these two developmental stages at the transcript level, with expression in Mo17 being higher for plastid ribosomal genes and B73 being higher for photosynthesis-related genes (Figure S6D). At the protein level, however, there is a reversal of expression differences between the parents for plastid ribosomal proteins (Figure S6C); B73 is the high parent in the seedling leaf, but Mo17 becomes the high parent in the leaf blade, revealing developmental-specific, post-transcriptional regulation. Interestingly, despite this flip in protein expression levels between these two growth stages in the parents, expression of plastid ribosomal proteins in the hybrid was consistently above mid-parent.

Correlations Between Plant Height Heterosis and Plastid Ribosome Expression Heterosis

To quantitatively characterize the relationship between phenotypic heterosis and protein expression heterosis in hybrids, we examined a set of nine hybrids made by back-crossing four recombinant inbred lines (RILs), derived from B73xMo17, to their two parents; and we included the parental hybrid, B73xMo17. The RIL hybrids were approximately 50% as heterozygous as

the parent hybrid and were selected based on their varied levels of plant height heterosis (Supplemental Data Set 2 and Supplemental Table 1).

We examined collectively the RIL hybrid set and the six hybrids described above to quantitatively assess correlations between expression heterosis and trait heterosis. Expression heterosis (hybrid level/MP level) of some protein complexes and pathways was strongly correlated with plant height heterosis (hybrid height/MP height) (Supplemental Data Set 3). Of the top 1.5% of proteins whose expression heterosis was most correlated with plant height heterosis, eighteen out of fifty-four were from the plastid ribosome (Table 1). Pearson's correlations of 0.79-0.91 were observed for these proteins, half of which were nuclear-encoded and half were plastid-encoded. Pearson correlations between protein expression heterosis and plant height heterosis were most positive for the plastid ribosomal proteins, slightly less positive for the cytosolic ribosomal proteins, and moderately positive for the PhANG/PhAPG proteins (Figure 2). The remaining proteins with positive correlations were not obviously related in function. No obvious functional enrichment was found for proteins with negative correlations. The analysis of RNAs revealed a different trend; expression heterosis of nuclear transcripts for the plastid ribosome was less correlated than their proteins with plant height heterosis; PhANG transcripts were substantially more positively correlated than their proteins; and transcripts for the cytosolic ribosome had no correlation (Figure 2 and Supplemental Data Set 3).

Accession	Pearson	Group
Zm00001d030725_T003	0.95	Plastid
Zm00001d022115_T002	0.92	Other
Zm00001d011993_T002	0.91	NE plastid ribosome
ZemaCp004.1	0.90	PE plastid ribosome
Zm00001d046555_T001	0.90	Plastid
ZemaCp016.1	0.90	PE plastid ribosome
Zm00001d050551_T001	0.89	Other
Zm00001d052075_T001	0.89	Cytosolic ribosome
Zm00001d054107_T002	0.87	Other
Zm00001d027442_T001	0.86	NE plastid ribosome
Zm00001d022421_T001	0.86	Other
Zm00001d012353_T001	0.86	NE plastid ribosome
Zm00001d053713_T001	0.86	Plastid

Zm00001d039613_T002	0.86	Other
Zm00001d052056_T005	0.85	Other
Zm00001d032399_T001	0.85	Other
Zm00001d029201_T001	0.84	NE plastid ribosome
Zm00001d049945_T004	0.84	Other
ZeamMp129.1	0.84	Other
ZemaCp021.1	0.84	PE plastid ribosome
Zm00001d013034_T001	0.84	Cytosolic ribosome
Zm00001d035802_T007	0.84	Other
Zm00001d036565_T001	0.84	Cytosolic ribosome
ZemaCp026.1	0.83	PE plastid ribosome
Zm00001d026690_T001	0.83	Other
Zm00001d015300_T001	0.83	Cytosolic ribosome
ZeamMp081.1	0.83	Other
Zm00001d041036_T001	0.83	Other
Zm00001d044880_T001	0.82	Other
Zm00001d013040_T008	0.82	Other
Zm00001d042454_T001	0.82	Plastid
Zm00001d028240_T001	0.82	NE plastid ribosome
Zm00001d042023_T001	0.82	Other
Zm00001d018412_T001	0.82	NE plastid ribosome
Zm00001d017449_T001	0.81	Plastid
Zm00001d015204_T001	0.81	NE plastid ribosome
ZemaCp058.1	0.81	PE plastid ribosome
Zm00001d047581_T002	0.81	NE plastid ribosome
Zm00001d016276_T001	0.81	Other
Zm00001d043465_T011	0.80	Other
Zm00001d032790_T002	0.80	Other
ZemaCp063.1	0.80	PE plastid ribosome
Zm00001d029968_T001	0.80	Other
ZemaCp062.1	0.80	PE plastid ribosome
Zm00001d022599_T001	0.80	Other
ZemaCp061.1	0.80	PE plastid ribosome
Zm00001d014519_T001	0.80	Other
ZeamMp119.1	0.80	Other
Zm00001d038006_T001	0.80	Other
Zm00001d043170_T001	0.79	Other
ZemaCp046.1	0.79	PE plastid ribosome
Zm00001d038851_T001	0.79	Other

Zm00001d037875_T001	0.79	Other
Zm00001d047462_T001	0.79	NE plastid ribosome

Table 1. The top 1.5% of proteins whose expression heterosis was most correlated with plant height heterosis. Data shown are Pearson correlations.

Reduced Levels of Ethylene Biosynthesis Enzymes Mediate the Hybrid Molecular Phenotypes

Of the three enzymes in the ET biosynthesis pathway, mutants in two of the maize genes encoding ACC synthase have been functionally characterized (*Zmacs2* and *Zmacs6*) as have four in Arabidopsis (*Ataco1*, *Ataco2*, *Atsams1*, and *Atsams2*). These mutants have decreased endogenous ET production (Cheng et al., 2009; Mao et al., 2015; Park et al., 2018; Young et al., 2004). While neither the AtACO1 homolog nor the ZmACS6 proteins/transcripts were detected in our results, we found that the AtACO2 homolog and AtSAM1/2 homolog gene transcripts and proteins, as well as the ZmACS2 gene transcript, were expressed substantially below mid-parent levels in the hybrid, B73xMo17 (Figure S7). Several other isoforms of the enzymes predicted to be involved in ET biosynthesis were also expressed significantly below mid-parent levels, although it remains unclear if reduced expression of these enzymes causes a reduction in ET levels. To investigate whether the reduced levels of transcripts/proteins for ET biosynthetic enzymes might mediate the dominant/overdominant expression of digenomic proteins in maize hybrids, we examined an ET biosynthesis double mutant (*Zmacs2/6*) in the B73 genetic background (Young et al., 2004). The hybrid molecular phenotype was partially phenocopied in leaves of the ET mutant (Figure 3). Levels of plastid ribosomal proteins were elevated in the mutant compared to B73 at the same proportion as in hybrids compared to mid-parent values. This indicates that reduced ET levels may mediate (1) the differences between inbreds and their hybrids and; (2) the differences between hybrids with varying levels of heterosis. PhANG and PhAPG proteins were also elevated in the mutant, although not to the extent typically seen in the hybrids. Expression levels of jasmonic acid (JA) biosynthesis enzymes were reduced in the *Zmacs2/6* mutant compared to B73 and in the hybrid B73xMo17 compared to MP levels (Figure S8 and Supplemental Table 2). Repression of JA biosynthetic protein levels appears to be caused by reduced ET synthesis, and this raises the possibility that JA may also play a role in the heterosis phenotypes.

Discussion

We report the first molecular phenotypes that are quantitatively associated with heterosis. Expression heterosis of the plastid ribosome displayed a strikingly positive correlation with plant height heterosis across a set of 15 hybrids (median Pearson correlation of 0.75 for proteins and 0.64 for RNAs). Only by comparing molecular and phenotypic parameters among a diverse set of hybrids were we able to discover the relationships between expression heterosis and growth heterosis. It is important to note that there was no correlation between expression levels and plant height; only the hybrid/MP values of each were correlated, while hybrid/HP values were weakly correlated. Ribosomal subunits were expressed at varying levels relative to MP, typically above but sometimes below, revealing a strong positive correlation to plant height heterosis. In contrast, hybrids expressed PhAPG and PhANG proteins above MP levels to similar relative amounts whether the hybrid displayed high or low levels of heterosis. As such, expression heterosis of the PhAPG and PhANG proteins was only moderately positively correlated with plant height heterosis (median Pearson correlation of 0.36 for proteins and 0.61 for RNAs). Expression heterosis at the protein level was correlated with expression heterosis at the RNA level for the plastid ribosomal proteins but not for the PhANGs (Figure S9). This explains the similarly positive correlations to plant height heterosis observed for the plastid ribosome, as well as the discrepancy observed for the PhANGs (Figure 2). The lack of correlation between RNAs and proteins for the PhANGs may be due to the rapid turnover of these proteins, as well as translational regulation.

We hypothesize that expression of the PhAPGs and PhANGs above MP levels increases photosynthesis and provides the added energy and carbon required for plant height heterosis. Coupling of photosynthesis to growth - specifically, the heterosis portions of each - may be through the plastid ribosome. Increased abundance of the plastid ribosome may enable higher levels and more rapid turnover of the PhANGs and PhAPGs, thereby reducing the effects of photoinhibition. Similar phenomena have been reported in yeast, where proteome reallocation from amino acid biosynthesis to ribosome biosynthesis enables yeast to grow faster in rich media (Björkeroth et al., 2020). The PhAPG and PhANG complexes can be rate-limiting for photosynthesis (Ermakova et al., 2019). Hybrids have increased rates of photosynthesis (Ko et al., 2016), which may be essential for heterosis of traits such as final plant biomass. A modest

gain of 10-20% should be more than enough to double the final plant biomass if cell numbers are compounded over time (Kelvin & Station, 1919).

Our results provide evidence for two genetic mechanisms of heterosis in maize. Both could contribute to high levels of macromolecular complexes, including the digenomic complexes required for photosynthesis and plastid protein synthesis. The first mechanism is based on genetic complementation between inbreds. A fixed stoichiometry of subunits in protein complexes implies that at least one subunit will be in limiting amounts, constraining the number of intact, functional complexes. Complementation can occur when the subunits in limiting amounts are different in each inbred. More copies of every subunit are incorporated into complexes in the hybrid because genetic complementation raises the levels of assembly-limiting subunits from each parent. The same argument holds for flux through multi-enzyme pathways, even if they are not organized as protein complexes. The inbred B73 was the high parent for relative expression of a majority of photosynthesis and plastid protein synthesis subunits and Mo17 was high parent for some. Low-parent and high-parent alleles are designated based on their relative expression between inbreds. We hypothesize that low-parent alleles for one or more genes express subunits in limiting amounts for that parent. Relative expression between inbreds can be reversed depending on the tissue and stage of development such that an allele is low-parent in one sample and high-parent in another (Zhou et al., 2019). Thus, heterosis should be possible with only MP levels of expression as long as there is complementation between genes in the same protein complex or pathway. Genetic complementation is related to the gene balance hypothesis, which explains how subunit stoichiometry may be altered by changes in chromosome copy number, leading to unbalanced protein subunit ratios that impair functionality (Birchler & Veitia, 2012; M. J. Song et al., 2020). We applied these concepts to differences in stoichiometry arising from allelic variation, rather than gene dosage. The gene balance hypothesis predicts that physiology may be impaired by unincorporated complex subunits. Our hypothesis doesn’t address this point directly and it suggests that the difference in vigor between inbreds and hybrids arises from the over-dominant cell copy number of intact complexes or pathways for photosynthesis and protein synthesis.

The second mechanism by which heterosis can arise is through over-dominant expression of protein subunits due to hybrid-specific increases in expression. In the hybrid, B73xMo17, we observed dominant expression of the chloroplast ribosomes and over-dominant expression of photosynthesis proteins. The levels of the ribosomal proteins varied across a set of diverse hybrids in proportion to phenotypic heterosis, whereas the levels of the photosynthesis proteins were always over-dominant. We hypothesize that over-dominant levels of photosynthesis proteins enable heterosis, and the specific levels of plastid ribosomes determines the quantity of heterosis. Combining genetic complementation with over-dominant expression levels may synergistically increase the numbers of functional protein complexes. It is conceivable that increased levels of subunits which are normally present in limiting amounts enable higher levels of all the other subunits to accumulate as members of a complex, whereas non-incorporated, unneeded subunits are rapidly degraded. Independently, higher levels of plastid ribosomes in hybrids may increase replacement of photo-damaged subunits and, thus, enable higher levels of active light reaction proteins. While we have focused our analyses on digenomic protein complexes in the chloroplast, other proteins and pathways in our data also exhibit over-dominant expression patterns or genetic complementation and they could be contributors to heterosis.

Our results combined with previous reports indicate that plastid digenomic protein expression differences between inbreds and hybrids are partially mediated by reduced ET biosynthetic gene expression. Maize *acs2* and *acs6* mutants are known to have improved leaf performance and elevated levels of foliar chlorophyll, Rubisco, and soluble protein (Young et al., 2004), which is reminiscent of the hybrid phenotype. Previous reports showed that nuclear-encoded plastid ribosomal protein gene transcription is highly responsive to stress (Sormani et al., 2011). It is conceivable that the reduced basal expression of stress-response genes in hybrids may contribute to the elevated expression of nuclear-encoded plastid ribosomes. However, while PhANG and PhAPG proteins were elevated in the *acs2-6* mutant (Figure 3), the trend was not as strong as observed in most hybrids. Additionally, the mutant does not display increased plant height. These observations suggest that other mechanisms, such as genetic complementation, may be necessary for plant height heterosis. Alternatively, it is possible that reduced ET levels in the mutant impair vigor in non-green tissues, whereas reduced ET is tissue-specific in the hybrid. Interestingly, the observation of down-regulated ET biosynthesis in hybrids has been reported in

Arabidopsis as well (Q. Song et al., 2018), suggesting there may be conserved mechanisms for hybrid vigor between monocots and dicots.

Methods

Plant growth and sampling

Plant materials were all grown in the green house for collection of seedling tissues and grown in the field for collection of adult tissues. The seedling leaf and mature leaf blade tissues of B73, Mo17 and B73xMo17 were collected in May of 2016 in St Paul, Minnesota, while tissues from the six hybrids and RIL hybrids experiments were collected from July to November of 2019 in St Paul, Minnesota. For seedling tissues, seeds were imbibed for 24 hours in distilled water and grown in growth chambers at 25°C under 12h light-dark cycles to V2/V3 stage (day 9) for collection of the V2 leaves. Tissue from at least four plants was pooled for each replicate and the three biological replicates were sampled at the same time (12PM) on different dates in order to sample the same growth stage for each genotype. For the *acs2/6* mutant and B73 seedling leaf samples, seeds were imbibed for 48 hours and manually examined to select uniformly germinating seedlings based on radical emergence and the lack of mold. They were then grown in growth chambers at 25°C under 12h light-dark cycles to V2/V3 stage (day 10). The V3 leaf was collected for 5 biological replicates of each genotype.

RNA-Seq analysis

Sequence libraries were prepared using the standard TruSeq Stranded mRNA library protocol and sequenced on NovaSeq 150bp paired end S4 flow cell to produce at least 20 million reads for each sample (Table S1). Both library construction and sequencing were done in the University of Minnesota Genomics Center. Sequencing reads were then processed through the nf-core RNA-Seq pipeline (Ewels et al., 2020) for initial QC and raw read counting. In short, reads were trimmed by Trim Galore! (https://github.com/FelixKrueger/TrimGalore) and aligned to the B73 maize reference genome (Zm-B73-REFERENCE-GRAMENE-4.0) (Jiao et al., 2017) using the variant-aware aligner Hisat2 (Kim et al., 2015) which also takes 90 million common variants to account for mapping bias. Uniquely aligned reads were then counted per feature by featureCounts (Liao et al., 2014). Raw read counts were then normalized by library size and corrected for library composition bias using the TMM normalization approach (Robinson &

Oshlack, 2010) to give CPMs (Counts Per Million reads) for each gene in each sample, allowing direct comparison across samples. CPM values were then normalized by gene CDS lengths to give FPKM (Fragments Per Kilobase of exon per Million reads) values. Hierarchical clustering, principal component analysis and t-SNE clustering were used to explore sample cluster patterns and to remove or substitute bad replicates.

Proteomics Sample Preparation

Ground tissue powders were suspended in extraction buffer (8M Urea/100mM Tris/5mM Tris(2-carboxyethyl)phosphine (TCEP)/phosphatase inhibitors, pH 7). Proteins were precipitated by adding 4 volumes of cold acetone and incubated at 4oC for 2 hours. Samples were centrifuged at 4,000xg, 4oC for 5 minutes. Supernatant was removed and discarded. Proteins were re-suspended in Urea extraction buffer (8M Urea/100mM Tris/5mM TCEP/phosphatase inhibitors, pH 7) and precipitated by cold acetone one more time. Protein pellets were washed by cold methanol to further remove non-protein contaminants. Protein pellets were suspended in extraction buffer (8M Urea/100mM Tris/5mM TCEP/phosphatase inhibitors, pH 7). Proteins were first digested with Lys-C (Wako Chemicals, 125-05061) at 37oC for 15 minutes. Protein solution was diluted 8 times to 1M urea with 100mM Tris and digested with trypsin (Roche, 03 708 969 001) for 4 hours. Digested peptides were purified on a Waters Sep-Pak C18 cartridges, eluted with 60% acetonitrile. TMT-10 labeling was performed in 50% acetonitrile/150mM Tris, pH7. TMT labeling efficiency was checked by LC-MS/MS to be greater than 99%. Labeled peptides from different samples (Table 3) were pooled together for 2D-nanoLC-MS/MS analysis. An Agilent 1100 HPLC system was used to deliver a flow rate of 600 nL min-1 to a custom 3-phase capillary chromatography column through a splitter. Column phases were a 20 cm long reverse phase (RP1, 5 µm Zorbax SB-C18, Agilent), 6 cm long strong cation exchange (SCX, 3 µm PolySulfoethyl, PolyLC), and 20 cm long reverse phase 2 (RP2, 3.5 µm BEH C18, Waters), with the electrospray tip of the fused silica tubing pulled to a sharp tip (inner diameter <1 µm). Peptide mixtures were loaded onto RP1, and the 3 sections were joined and mounted on a custom electrospray adapter for on-line nested elutions. Peptides were eluted from RP1 section to SCX section using a 0 to 80% acetonitrile gradient for 60 minutes, and then were fractionated by the SCX column section using a series of 20 step salt gradients of ammonium acetate over 20 min,

followed by high-resolution reverse phase separation on the RP2 section of the column using an acetonitrile gradient of 0 to 80% for 150 minutes.

Proteomics data acquisition

Spectra are acquired on a Q-exactive-HF mass spectrometer (Thermo Electron Corporation, San Jose, CA) operated in positive ion mode with a source temperature of 275 °C and spray voltage of 3kV. Automated data-dependent acquisition was employed of the top 20 ions with an isolation windows of 1.0 Da and collision energy of 30. The mass resolution is set at 60,000 for MS and 30,000 for MS/MS scans, respectively. Dynamic exclusion is used to improve the duty cycle.

Proteomics data analysis

The raw data was extracted and searched using Spectrum Mill vB.06 (Agilent Technologies). MS/MS spectra with a sequence tag length of 1 or less were considered to be poor spectra and were discarded. The remaining high quality MS/MS spectra were searched against a maize protein database including maize B73 (Zm-B73-REFERENCE-GRAMENE-4.0) and Mo17 (Zm-Mo17-REFERENCE-CAU-1.0) reference genomes (Jiao et al., 2017; Sun et al., 2018). A 1:1 concatenated forward-reverse database was constructed to calculate the false discovery rate (FDR). There were 435,212 protein sequences in the final protein database. Search parameters were set to Spectrum Mill's default settings with the enzyme parameter limited to full tryptic peptides with a maximum mis-cleavage of 1. Cutoff scores were dynamically assigned to each dataset to obtain the false discovery rates (FDR) of 0.1% for peptides, and 1% for proteins. Proteins that share common peptides were grouped using principles of parsimony to address protein database redundancy. Total TMT-10 reporter intensities were used for relative protein quantitation. Peptides shared among different protein groups were removed before TMT quantitation. Isotope impurities of TMT-10 reagents were corrected using correction factors provided by the manufacturer (Thermo). Median normalization was performed to normalize the protein TMT-10 reporter intensities in which the log ratios between different TMT-10 tags were adjusted globally such that the median log ratio was zero.

Proteomics data deposition

The raw spectra for the proteome data have been deposited in the Mass Spectrometry Interactive Virtual Environment (MassIVE) repository (massive.ucsd.edu/ProteoSAFe/static/massive.jsp) (accession ID MSV000085916). FTP download link before publication: ftp://MSV000085916@massive.ucsd.edu; FTP download link after publication: ftp://massive.ucsd.edu/MSV000085916/.

Expression analysis

For protein analyses, tandem-mass tag (TMT) abundances were normalized to the arithmetic mean of the B73 replicates in each run (Supplemental Data Set 5). For RNA analysis of the original seedling leaf and leaf blade, previously published counts per million (CPM) values were used (Zhou et al., 2019) For six hybrid and RIL hybrid RNA analyses, CPM values were used (Supplemental Data Sets 6 and 7 for six hybrids and RIL hybrids, respectively). For each experiment, genes or proteins were removed if they were not detected in all biological replicates. The arithmetic mean of the biological replicates was then calculated and used to calculate hybrid/mid-parent and parent/parent ratios. The log base 2 was then calculated for each ratio. Data was manipulated using the R packages dplyr (Wickham et al., 2019), plyr (Wickham, 2011), tidyr (Wickham & Henry, 2019), reshape2 (Wickham, 2007), and data.table (Dowle & Srinivasan, 2019). Scatterplots were generated using ggplot2 (Wickham, 2016), density plots were generated using cowplot (Wilke, 2019), and plots were assembled into paneled figures using patchwork (Pedersen, 2019). Coefficients of variation were calculated using EnvStats (Millard, 2013) and plots were generated using ggplot2 (Wickham, 2016). For correlation analyses, the Pearson correlation was calculated from the hybrid/mid-parent or hybrid/BxM expression ratios to the hybrid/mid-parent plant height ratios (Supplemental Table 1) and plotted using ggridges (Wilke, 2020). KEGG maps were generated using pathview (Luo & Brouwer, 2013) and mapping data was exported (Supplemental Table 2).

Protein group assignment

The plastid proteome was defined according to a previous report (Friso et al., 2010). PhANGs were defined using KEGG zma00195, excluding the electron transport proteins, zma00196, and CornCyc reactions 1.97.1.12 and 1.10.3.9 (Kanehisa, 2019; Portwood et al., 2019), all of which were downloaded on February 26, 2020. The PhAPGs were defined as the plastid-encoded

proteins in PSI, PSII, cytochrome b6f, and ATP synthase. Nuclear-encoded plastid ribosomal proteins were defined as those containing "30S" or "50S" in their NCBI annotation as well as "plastid" or "chloroplast" in their maize-GAMER GO annotations (Wimalanathan et al., 2018), with term descriptions retrieved using the R package AnnotationDbi (Pagès et al., 2019). Cytosolic ribosomal proteins were defined as those containing "40S" or "60S" in their NCBI annotation, except for those containing "mitochondrial" or "biogenesis". Ethylene biosynthetic proteins were defined using CornCyc reactions 2.5.1.6, 4.4.1.14 and 1.14.17.4 (Portwood et al., 2019), downloaded on May 5, 2020. All accession conversions were made using the MaizeGDB accession conversion table, downloaded on May 18, 2020 (Portwood et al., 2019). A complete list of gene group assignments and their sources is provided in Supplemental Table 6.

Code availability

All source codes used for expression analyses are available on Github: https://github.com/devonbirdseye/HeterosisManuscript

Funding

This material is based upon work supported by the National Science Foundation Grant No. 1546899 to S.P.B and N.M.S., and the National Science Foundation Graduate Research Fellowship under Grant No. DGE-1650112 to D.B. Any opinions, findings, and conclusions or recommendations expressed in this material are those of the authors and do not necessarily reflect the views of the National Science Foundation.

Author Contributions

S.P.B., N.M.S., L.D., Z.S., and D.B. conceived the experiments. Z.S., D.B. and P.Z. performed the experiments. D.B. performed the data analysis and developed visualizations of data. S.P.B and D.B. wrote the paper. E.A.S. and H.B. provided expertise, ideas, and feedback.

References

Birchler, J. A., & Veitia, R. A. (2012). Gene balance hypothesis: Connecting issues of dosage sensitivity across biological disciplines. *Proceedings of the National Academy of Sciences of the United States of America*, *109*(37), 14746–14753. https://doi.org/10.1073/pnas.1207726109

Björkeroth, J., Campbell, K., Malina, C., Yu, R., Di Bartolomeo, F., & Nielsen, J. (2020). Proteome reallocation from amino acid biosynthesis to ribosomes enables yeast to grow

faster in rich media. *Proceedings of the National Academy of Sciences*, *117*(35), 201921890. https://doi.org/10.1073/pnas.1921890117

Cheng, W. H., Chiang, M. H., Hwang, S. G., & Lin, P. C. (2009). Antagonism between abscisic acid and ethylene in Arabidopsis acts in parallel with the reciprocal regulation of their metabolism and signaling pathways. *Plant Molecular Biology*, *71*(1–2), 61–80. https://doi.org/10.1007/s11103-009-9509-7

Dahal, D., Newton, K. J., & Mooney, B. P. (2016). Quantitative proteomics of Zea mays hybrids exhibiting different levels of heterosis. *Journal of Proteome Research*, *15*(8), 2445–2454. https://doi.org/10.1021/acs.jproteome.5b01120

Dowle, M., & Srinivasan, A. (2019). *data.table: Extension of `data.frame`* (R package version 1.12.2). https://cran.r-project.org/package=data.table

Dudley, J. W., Maroof, M. A. S., & Rufener, G. K. (1991). Molecular Markers and Grouping of Parents in Maize Breeding Programs. *Crop Science*, *31*(3). https://doi.org/10.2135/cropsci1991.0011183X003100030036x

Ermakova, M., Lopez-calcagno, P. E., Caemmerer, S. Von, Raines, C. A., & Furbank, R. T. (2019). Overexpression of the Rieske FeS protein of the Cytochrome b 6 f complex increases. *Communications Biology*, *2*(314), 1–12. https://doi.org/10.1038/s42003-019-0561-9

Ewels, P. A., Peltzer, A., Fillinger, S., Patel, H., Alneberg, J., Wilm, A., Garcia, M. U., Di Tommaso, P., & Nahnsen, S. (2020). The nf-core framework for community-curated bioinformatics pipelines. *Nature Biotechnology*, *38*(3), 276–278. https://doi.org/10.1038/s41587-020-0439-x

Friso, G., Majeran, W., Huang, M., Sun, Q., & van Wijk, K. J. (2010). Reconstruction of metabolic pathways, protein expression, and homeostasis machineries across maize bundle sheath and mesophyll chloroplasts: Large-scale quantitative proteomics using the first maize genome assembly. *Plant Physiology*, *152*(3), 1219–1250. https://doi.org/10.1104/pp.109.152694

Fujimoto, R., Taylor, J. M., Shirasawa, S., Peacock, W. J., & Dennis, E. S. (2012). *Heterosis of Arabidopsis hybrids between C24 and Col is associated with increased photosynthesis capacity*. *109*(18), 7109–7114. https://doi.org/10.1073/pnas.1204464109

Guo, B., Chen, Y., Zhang, G., Xing, J., Hu, Z., Feng, W., Yao, Y., Peng, H., Du, J., Zhang, Y.,

Ni, Z., & Sun, Q. (2013). Comparative Proteomic Analysis of Embryos between a Maize Hybrid and Its Parental Lines during Early Stages of Seed Germination. *PLoS ONE*, *8*(6). https://doi.org/10.1371/journal.pone.0065867

Habben, J. E., Bao, X., Bate, N. J., Debruin, J. L., Dolan, D., Hasegawa, D., Helentjaris, T. G., Lafitte, R. H., Lovan, N., Mo, H., Reimann, K., & Schussler, J. R. (2014). Transgenic alteration of ethylene biosynthesis increases grain yield in maize under field drought-stress conditions. *Plant Biotechnology Journal*, *12*(6), 685–693. https://doi.org/10.1111/pbi.12172

Haney WJ, Gartner JB, W. G. (1953). THE EFFECT OF LIGHT ON THE EXPRESSION OF HETEROSIS. *Journal of Heredity*, *44*(1), 10–12. https://doi.org/https://doi.org/10.1093/oxfordjournals.jhered.a106339

Hu, X., Wang, H., Li, K., Wu, Y., Liu, Z., & Huang, C. (2017a). Genome-wide proteomic profiling reveals the role of dominance protein expression in heterosis in immature maize ears. *Scientific Reports*, *7*(1), 1–12. https://doi.org/10.1038/s41598-017-15985-3

Hu, X., Wang, H., Li, K., Wu, Y., Liu, Z., & Huang, C. (2017b). Genome-wide proteomic profiling reveals the role of dominance protein expression in heterosis in immature maize ears. *Scientific Reports*, *7*(1). https://doi.org/10.1038/s41598-017-15985-3

Jiao, Y., Peluso, P., Shi, J., Liang, T., Stitzer, M. C., Wang, B., Campbell, M. S., Stein, J. C., Wei, X., Chin, C. S., Guill, K., Regulski, M., Kumari, S., Olson, A., Gent, J., Schneider, K. L., Wolfgruber, T. K., May, M. R., Springer, N. M., … Ware, D. (2017). Improved maize reference genome with single-molecule technologies. *Nature*, *546*(7659), 524–527. https://doi.org/10.1038/nature22971

Kanehisa, M. (2019). Toward understanding the origin and evolution of cellular organisms. *Protein Science*, *28*(11), 1947–1951. https://doi.org/10.1002/pro.3715

Kelvin, Lord, & Station, C. E. (1919). *The Compound Interest Law and Plant Growth. XXXIII*(Cxxxi).

Kim, D., Langmead, B., & Salzberg, S. L. (2015). HISAT: A fast spliced aligner with low memory requirements. *Nature Methods*, *12*(4), 357–360. https://doi.org/10.1038/nmeth.3317

Ko, D. K., Rohozinski, D., Song, Q., Taylor, S. H., Juenger, T. E., Harmon, F. G., & Chen, Z. J. (2016). Temporal Shift of Circadian-Mediated Gene Expression and Carbon Fixation Contributes to Biomass Heterosis in Maize Hybrids. *PLoS Genetics*, *12*(7), 1–31.

https://doi.org/10.1371/journal.pgen.1006197

Li, Z., Zhu, A., Song, Q., Chen, H. Y., Harmon, F. G., & Chen, Z. J. (2020). Temporal Regulation of the Metabolome and Proteome in Photosynthetic and Photorespiratory Pathways Contributes to Maize Heterosis. *The Plant Cell*, *32*(November), tpc.00320.2020. https://doi.org/10.1105/tpc.20.00320

Liao, Y., Smyth, G. K., & Shi, W. (2014). FeatureCounts: An efficient general purpose program for assigning sequence reads to genomic features. *Bioinformatics*, *30*(7), 923–930. https://doi.org/10.1093/bioinformatics/btt656

Luo, W., & Brouwer, C. (2013). Pathview: an R/Bioconductor package for pathway-based data integration and visualization. *Bioinformatics*, *29*(14), 1830–1831. https://doi.org/10.1093/bioinformatics/btt285

Mao, D., Yu, F., Li, J., Van de poel, B., Tan, D., Li, J., Liu, Y., Li, X., Dong, M., Chen, L., Li, D., & Luan, S. (2015). FERONIA receptor kinase interacts with S-adenosylmethionine synthetase and suppresses S-adenosylmethionine production and ethylene biosynthesis in Arabidopsis. *Plant Cell and Environment*, *38*(12), 2566–2574. https://doi.org/10.1111/pce.12570

Marcon, C., Lamkemeyer, T., Ahmed, W., Ungrue, D., Piepho, H., & Hochholdinger, F. (2013). Heterosis-associated proteome analyses of maize (Zea mays L.) seminal roots by quantitative label-free LC – MS ☆. *Journal of Proteomics*, *93*, 295–302. https://doi.org/10.1016/j.jprot.2013.04.015

Meyer, R. C., Molecular, M., Physiology, P., & Germany, R. C. M. (2004). *Heterosis of Biomass Production in Arabidopsis . Establishment during Early Development 1*. *134*(April), 1813–1823. https://doi.org/10.1104/pp.103.033001.hybrid

Millard, S. P. (2013). *EnvStats: An R Package for Environmental Statistics*. Springer-Verlag New York.

Pagès, H., Carlson, M., Falcon, S., & Li, N. (2019). *AnnotationDbi: Manipulation of SQLite-based annotations in Bioconductor* (R package version 1.46.1).

Park, C. H., Roh, J., Youn, J. H., Son, S. H., Park, J. H., Kim, S. Y., Kim, T. W., & Kim, S. K. (2018). Arabidopsis ACC oxidase 1 coordinated by multiple signals mediates ethylene biosynthesis and is involved in root development. *Molecules and Cells*, *41*(10), 923–932. https://doi.org/10.14348/molcells.2018.0092

Pedersen, T. (2019). *patchwork: The Composer of Plots* (R package version 1.0.0).

Portwood, J. L., Woodhouse, M. R., Cannon, E. K., Gardiner, J. M., Harper, L. C., Schaeffer, M. L., Walsh, J. R., Sen, T. Z., Cho, K. T., Schott, D. A., Braun, B. L., Dietze, M., Dunfee, B., Elsik, C. G., Manchanda, N., Coe, E., Sachs, M., Stinard, P., Tolbert, J., … Andorf, C. M. (2019). Maizegdb 2018: The maize multi-genome genetics and genomics database. *Nucleic Acids Research*, *47*(D1), D1146–D1154. https://doi.org/10.1093/nar/gky1046

Robinson, M. D., & Oshlack, A. (2010). A scaling normalization method for differential expression analysis of RNA-seq data. *Genome Biology*, *11*(3). https://doi.org/10.1186/gb-2010-11-3-r25

Rockenbach, M. F., Corrêa, C. C. G., Heringer, A. S., Freitas, I. L. J., Santa-Catarina, C., Do Amaral, A. T., & Silveira, V. (2018). Differentially abundant proteins associated with heterosis in the primary roots of popcorn. *PLoS ONE*, *13*(5). https://doi.org/10.1371/journal.pone.0197114

Rosenfield, J. A., Nolasco, S., Lindauer, S., Sandoval, C., & Kodric-Brown, A. (2004). The role of hybrid vigor in the replacement of pecos pupfish by its hybrids with sheepshead minnow. *Conservation Biology*, *18*(6), 1589–1598. https://doi.org/10.1111/j.1523-1739.2004.00356.x

Schnable, P. S., & Springer, N. M. (2013a). Progress Toward Understanding Heterosis in Crop Plants. *Annual Review of Plant Biology*, *64*(1), 71–88. https://doi.org/10.1146/annurev-arplant-042110-103827

Schnable, P. S., & Springer, N. M. (2013b). Progress toward understanding heterosis in crop plants. *Annual Review of Plant Biology*, *64*, 71–88. https://doi.org/10.1146/annurev-arplant-042110-103827

Song, M. J., Potter, B. I., Doyle, J. J., & Coate, J. E. (2020). Gene Balance Predicts Transcriptional Responses Immediately Following Ploidy Change in Arabidopsis thaliana *The Plant Cell*, *32*(5), 1434 LP – 1448. https://doi.org/10.1105/tpc.19.00832

Song, Q., Ando, A., Xu, D., Fang, L., Zhang, T., Huq, E., Qiao, H., Deng, X. W., & Jeffrey Chen, Z. (2018). Diurnal down-regulation of ethylene biosynthesis mediates biomass heterosis. *Proceedings of the National Academy of Sciences of the United States of America*, *115*(21), 5606–5611. https://doi.org/10.1073/pnas.1722068115

Song, Y., Zhang, Z., Tan, X., Jiang, Y., Gao, J., Lin, L., Wang, Z., Ren, J., Wang, X., Qin, L.,

Cheng, W., Qi, J., & Kuai, B. (2016). Association of the molecular regulation of ear leaf senescence/stress response and photosynthesis/metabolism with heterosis at the reproductive stage in maize. *Scientific Reports*, *6*(June), 1–12. https://doi.org/10.1038/srep29843

Sormani, R., Masclaux-Daubresse, C., Daniele-Vedele, F., & Chardon, F. (2011). Transcriptional regulation of ribosome components are determined by stress according to cellular compartments in Arabidopsis thaliana. *PLoS ONE*, *6*(12). https://doi.org/10.1371/journal.pone.0028070

Stupar, R. M., Gardiner, J. M., Oldre, A. G., Haun, W. J., Chandler, V. L., & Springer, N. M. (2008). Gene expression analyses in maize inbreds and hybrids with varying levels of heterosis. *BMC Plant Biology*, *8*, 33. https://doi.org/10.1186/1471-2229-8-33

Sun, S., Zhou, Y., Chen, J., Shi, J., Zhao, H., Zhao, H., Song, W., Zhang, M., Cui, Y., Dong, X., Liu, H., Ma, X., Jiao, Y., Wang, B., Wei, X., Stein, J. C., Glaubitz, J. C., Lu, F., Yu, G., … Lai, J. (2018). Extensive intraspecific gene order and gene structural variations between Mo17 and other maize genomes. *Nature Genetics*, *50*(9), 1289–1295. https://doi.org/10.1038/s41588-018-0182-0

Troyer, A. F. (2006). Adaptedness and heterosis in corn and mule hybrids. *Crop Science*, *46*(2), 528–543. https://doi.org/10.2135/cropsci2005.0065

Walley, J. W., Sartor, R. C., Shen, Z., Schmitz, R. J., Wu, K. J., Urich, M. A., Nery, J. R., Smith, L. G., Schnable, J. C., Ecker, J. R., & Briggs, S. P. (2016). Integration of omic networks in a developmental atlas of maize. *Science*, *353*(6301). https://doi.org/10.1126/science.aag1125

Walley, J. W., Shen, Z., Sartor, R., Wu, K. J., Osborn, J., Smith, L. G., & Briggs, S. P. (2013). Reconstruction of protein networks from an atlas of maize seed proteotypes. *Proceedings of the National Academy of Sciences of the United States of America*, *110*(49), E4808-17. https://doi.org/10.1073/pnas.1319113110

Wickham, H. (2007). Reshaping Data with the {reshape} Package. *Journal of Statistical Software*, *21*(12), 1–20.

Wickham, H. (2011). The Split-Apply-Combine strategy for data analysis. *J. Stat. Softw.*, *40*, 1–29. http://ci.nii.ac.jp/naid/20001506321/en/

Wickham, H. (2016). *ggplot2: Elegant Graphics for Data Analysis*. Springer-Verlag New York.

Wickham, H., François, R., Henry, L., & Müller, K. (2019). *dplyr: A Grammar of Data Manipulation* (R package version 0.8.3). https://cran.r-project.org/package=dplyr

Wickham, H., & Henry, L. (2019). *tidyr: Easily Tidy Data with "spread()" and "gather()" Functions*. https://cran.r-project.org/package=tidyr

Wilke, C. O. (2019). *cowplot: Streamlined Plot Theme and Plot Annotations for "ggplot2"* (R package version 1.0.0).

Wilke, C. O. (2020). *ggridges: Ridgeline Plots in "ggplot2"* (R package version 0.5.2).

Wimalanathan, K., Friedberg, I., Andorf, C. M., & Lawrence-Dill, C. J. (2018). Maize GO Annotation—Methods, Evaluation, and Review (maize-GAMER). *Plant Direct*, *2*(4), 1–15. https://doi.org/10.1002/pld3.52

Young, T. E., Meeley, R. B., & Gallie, D. R. (2004). ACC synthase expression regulates leaf performance and drought tolerance in maize. *Plant Journal*, *40*(5), 813–825. https://doi.org/10.1111/j.1365-313X.2004.02255.x

Zhou, P., Hirsch, C. N., Briggs, S. P., & Springer, N. M. (2019). Dynamic Patterns of Gene Expression Additivity and Regulatory Variation throughout Maize Development. *Molecular Plant*, *12*(3), 410–425. https://doi.org/10.1016/j.molp.2018.12.015

Zhou, P., Silverstein, K. A. T., Gao, L., Walton, J. D., Nallu, S., Guhlin, J., & Young, N. D. (2013). Detecting small plant peptides using SPADA (Small Peptide Alignment Discovery Application). *BMC Bioinformatics*, *14*(1). https://doi.org/10.1186/1471-2105-14-335

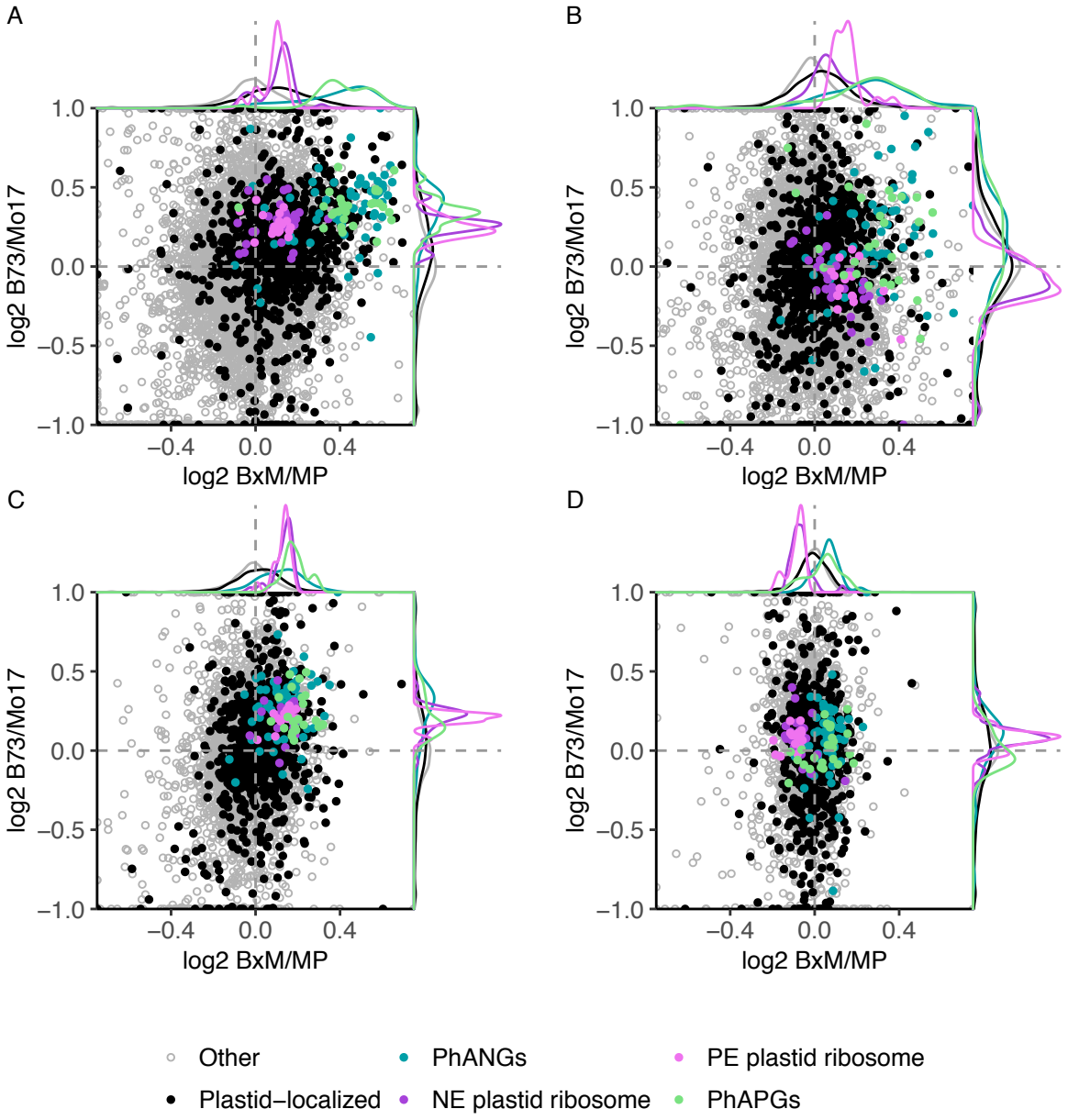

Fig 1. Ratios of plastid-localized proteins in leaves of inbred B73 to Mo17, and of hybrid B73xMo17 to mid-parent (MP) levels grown and analyzed in four independent experiments. Each data point is the mean of three biological replicates. A=seedling leaf from original experiment, B=mature leaf blade from original experiment, C=seedling leaf from six hybrids experiment, D= seedling leaf from RIL experiment. Photosynthesis-Associated Nuclear Genes (PhANGs), Photosynthesis-Associated Plastid Genes (PhAPGs), Plastid-Encoded (PE) plastid ribosomes and Nuclear-Encoded (NE) plastid ribosomes are color-coded.

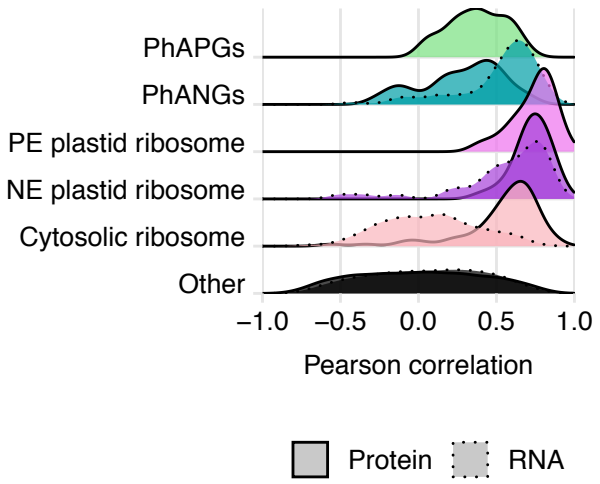

Figure 2. Density curves of Pearson correlations between protein expression heterosis and plant height heterosis in the combined RIL and six hybrids datasets

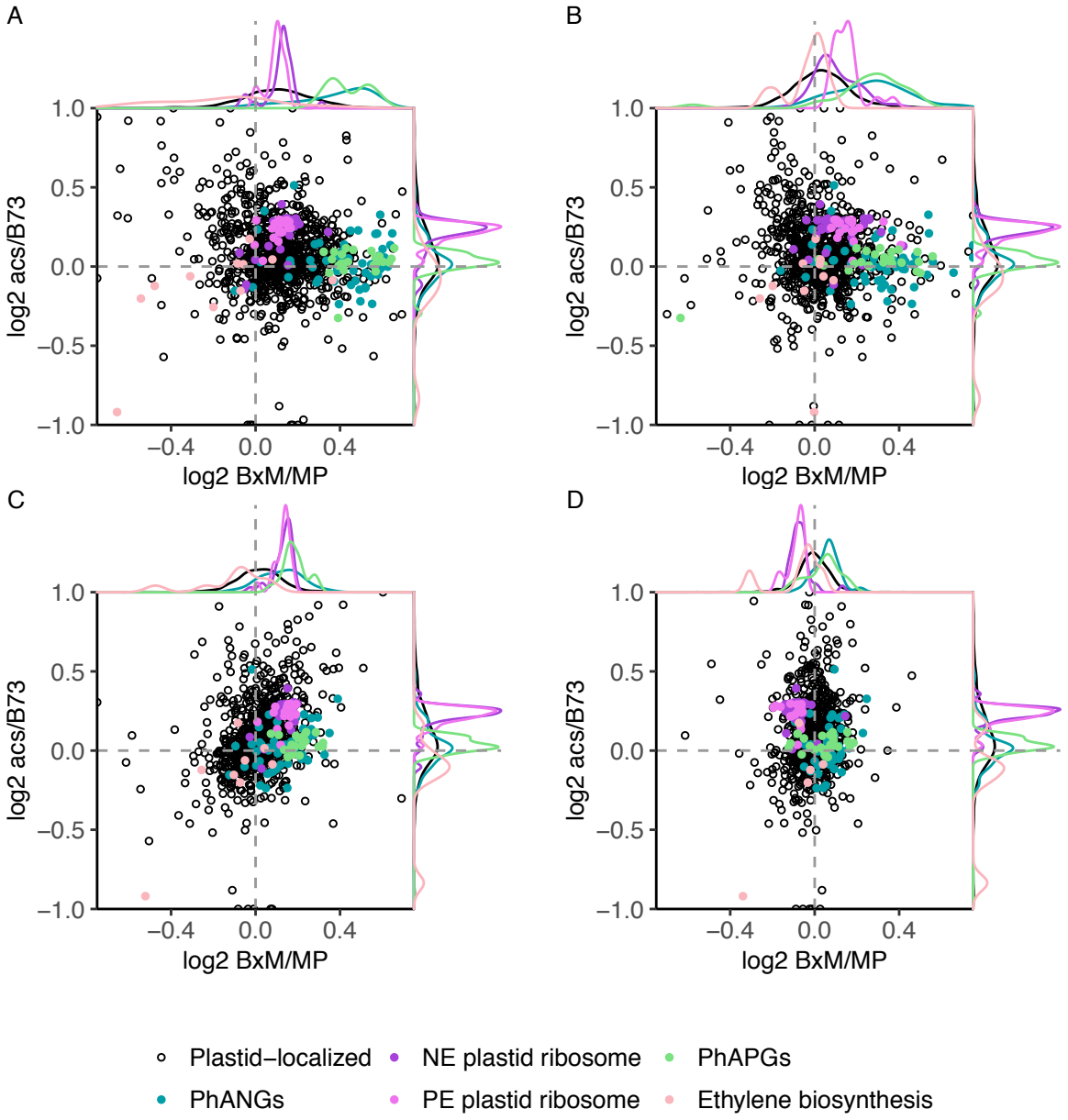

Fig 3. Plastid-localized proteins in seedling leaves of the *acs2-6* double mutant in B73 background relative to B73, compared to expression heterosis of the BxM hybrid from the seedling leaf from original experiment (A), the mature leaf blade from original experiment (B), the seedling leaf from six hybrids experiment (C), and the seedling leaf from RIL experiment (D). Each data point represents the mean of five biological replicates for *acs2-6*/B73 and three biological replicates for BxM/MP. Photosynthesis-Associated Nuclear Genes (PhANGs), Photosynthesis-Associated Plastid Genes (PhAPGs), Plastid-Encoded (PE) plastid ribosomes, Nuclear-Encoded (NE) plastid ribosomes, and ethylene biosynthesis proteins are color-coded.

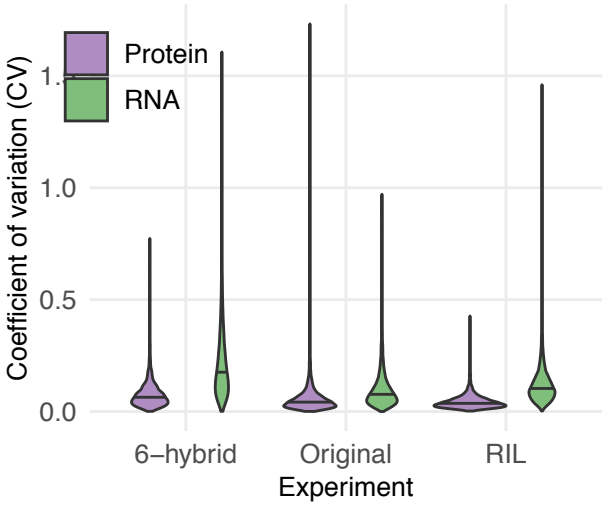

Supplemental Figure 1. Coefficients of variation of the three B73xMo17 seedling leaf biological replicates for proteins compared to their corresponding transcripts.

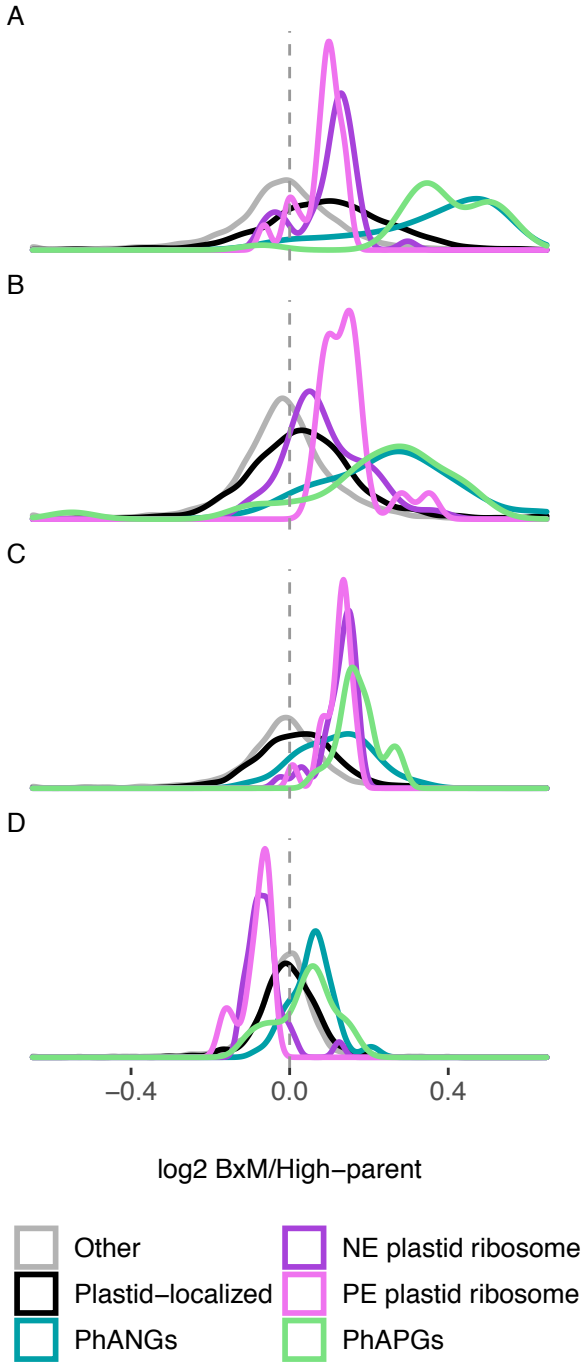

Supplemental Figure 2. Density curves corresponding to the ratios of plastid-localized proteins in leaves of hybrid B73xMo17 to high-parent levels, grown and analyzed in four independent experiments: A=seedling leaf from original experiment, B=mature leaf blade from original experiment, C=seedling leaf from six hybrids experiment, D= seedling leaf from RIL experiment. Photosynthesis-Associated Nuclear Genes (PhANGs), Photosynthesis-Associated Plastid Genes (PhAPGs), Plastid-Encoded (PE) plastid ribosomes and Nuclear-Encoded (NE) plastid ribosomes are color-coded.

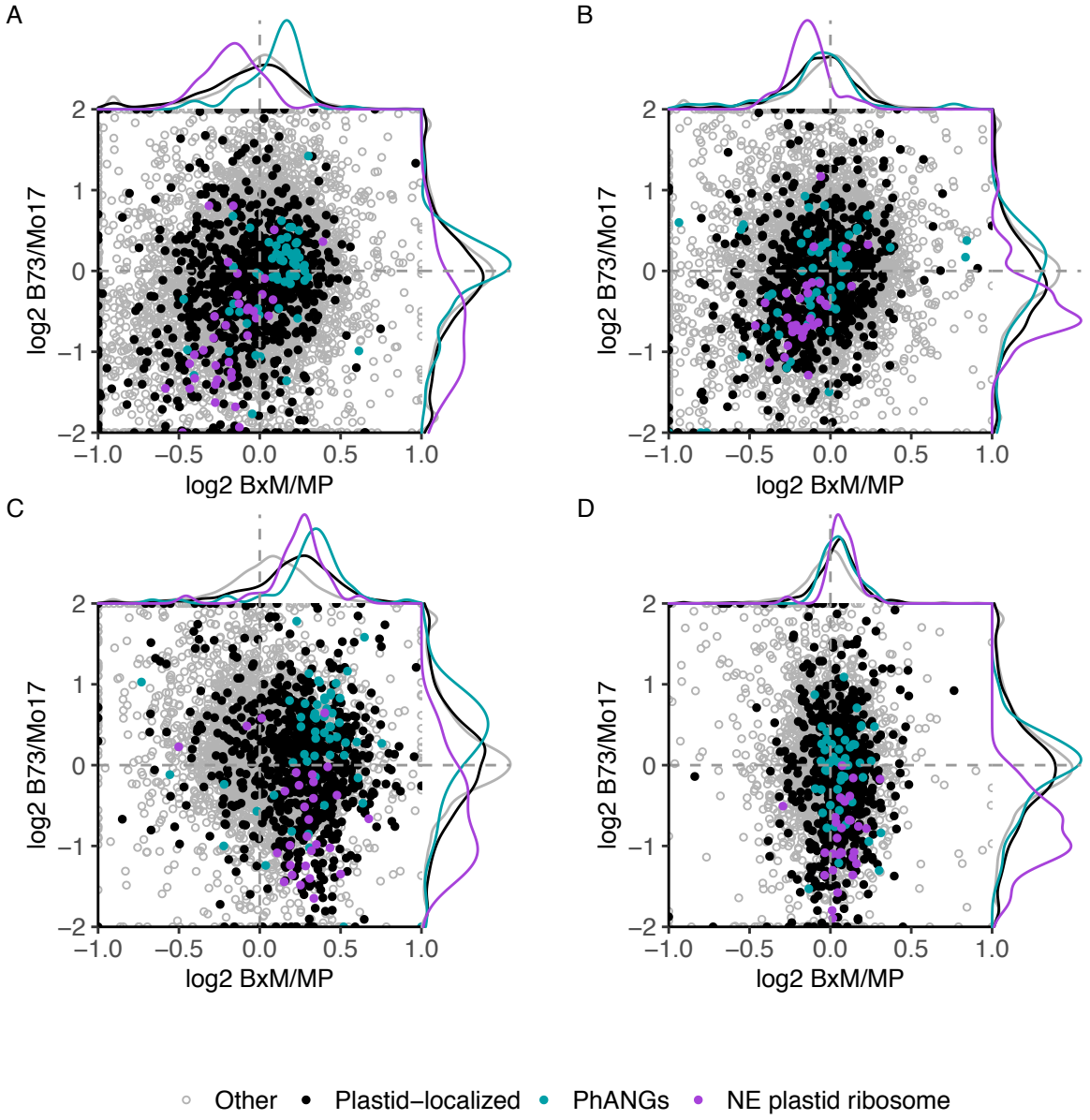

Supplemental Figure 3. Ratios of transcripts of plastid-localized proteins in leaves of inbred B73 to Mo17, and of hybrid B73xMo17 to mid-parent (MP) levels grown and analyzed in four independent experiments. Each data point is the mean of three biological replicates. Only transcripts for which a protein was detected are shown. A=seedling leaf from original experiment, B=mature leaf blade from original experiment, C=seedling leaf from six hybrids experiment, D= seedling leaf from RIL experiment. Photosynthesis-Associated Nuclear Genes (PhANGs) and Nuclear-Encoded (NE) plastid ribosomes are color-coded.

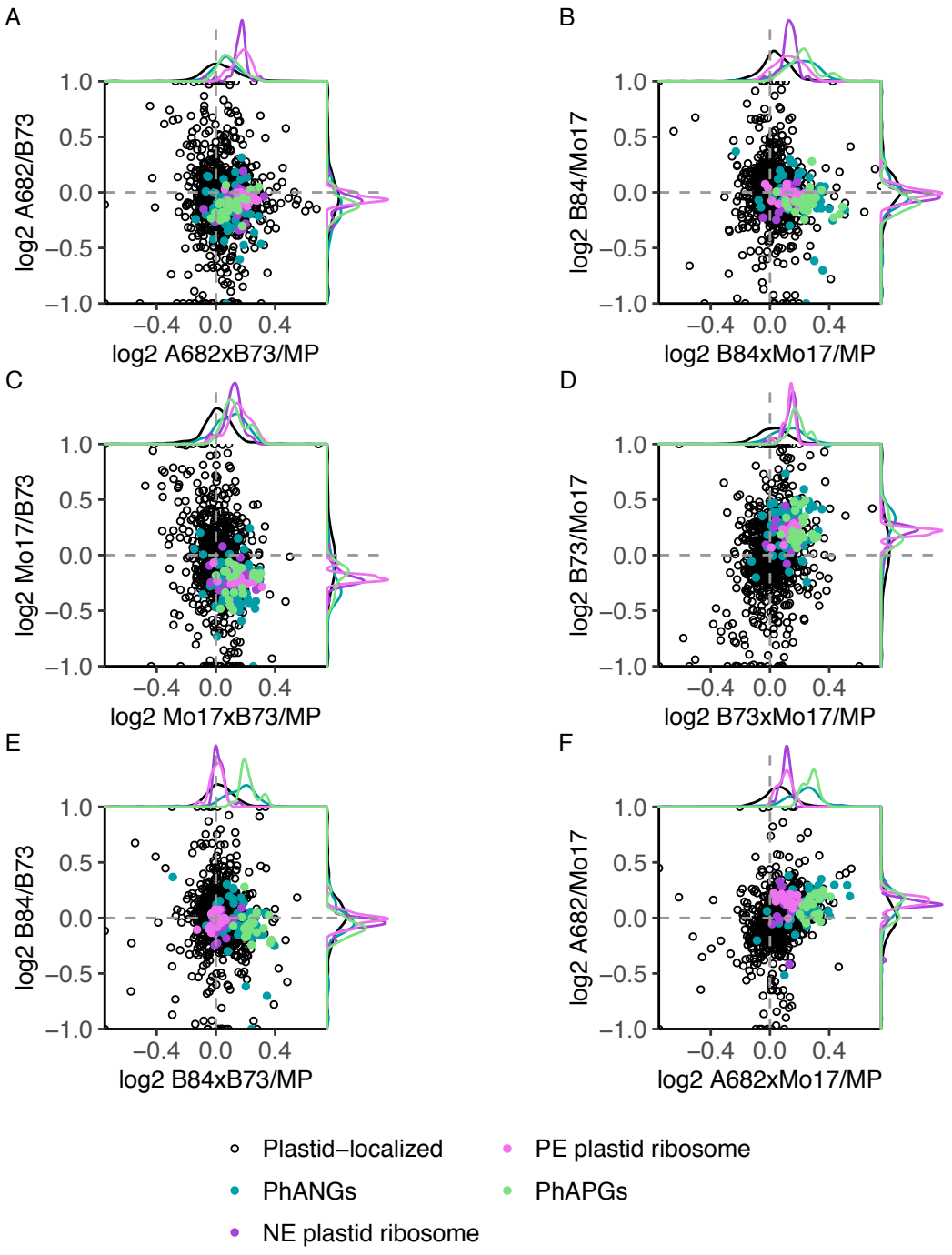

Supplemental Figure 4. Plastid-localized proteins in seedling leaves of six hybrids and their inbred parents. Hybrids represented in A-F are ordered from greatest plant height heterosis (A) to least plant height heterosis (F). Each data point is the mean of three biological replicates. Photosynthesis-Associated Nuclear Genes (PhANGs), Photosynthesis-Associated Plastid Genes (PhAPGs), Plastid-Encoded (PE) plastid ribosomes, and Nuclear-Encoded (NE) plastid ribosomes are color-coded.

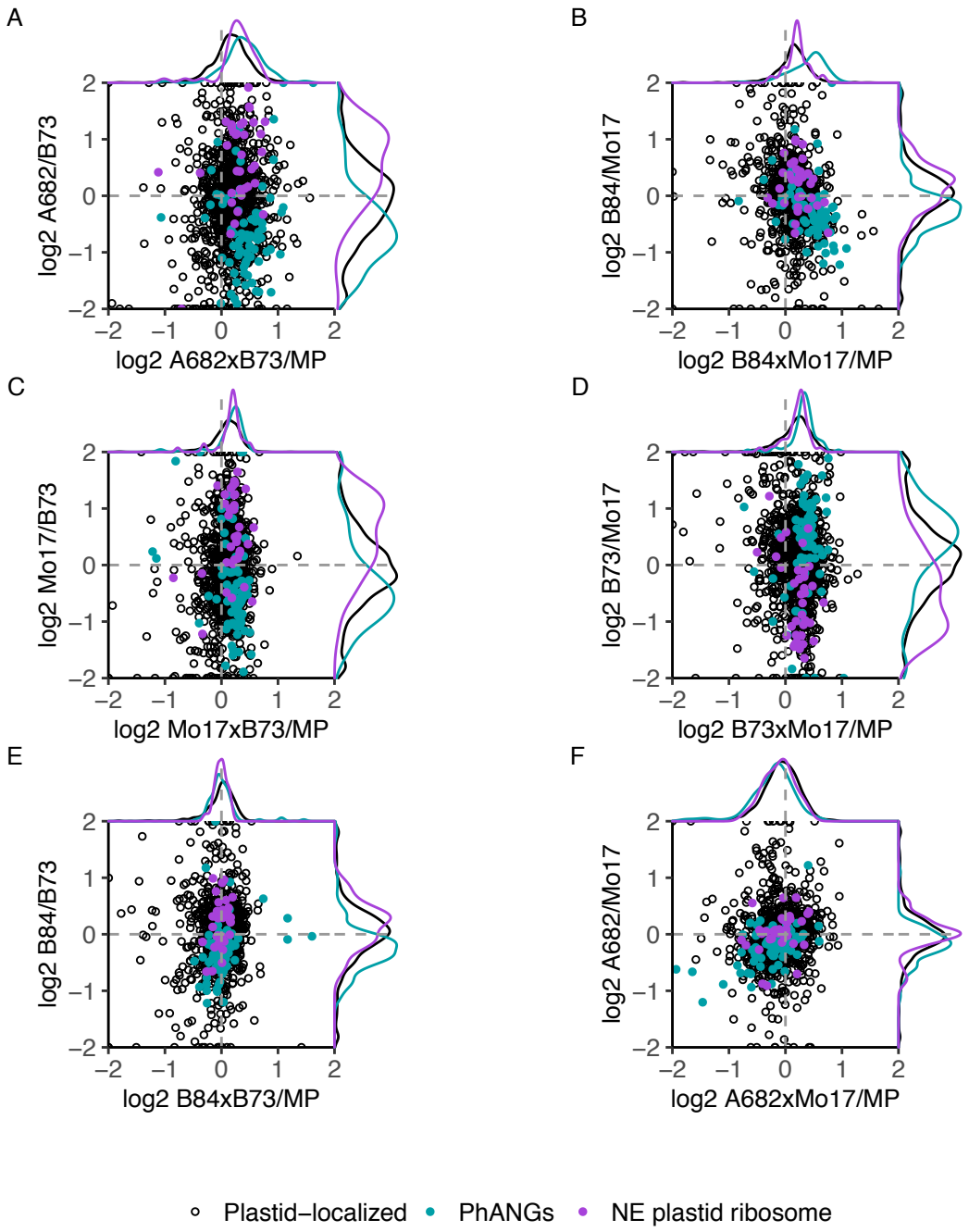

Supplemental Figure 5. Transcripts of plastid-localized proteins in seedling leaves of six hybrids. Hybrids represented in A-F are ordered from greatest plant height heterosis (A) to least plant height heterosis (F). Each data point is the mean of three biological replicates. Only transcripts for which a protein was detected are shown. Photosynthesis-Associated Nuclear Genes (PhANGs) and Nuclear-Encoded (NE) plastid ribosomes are color-coded.

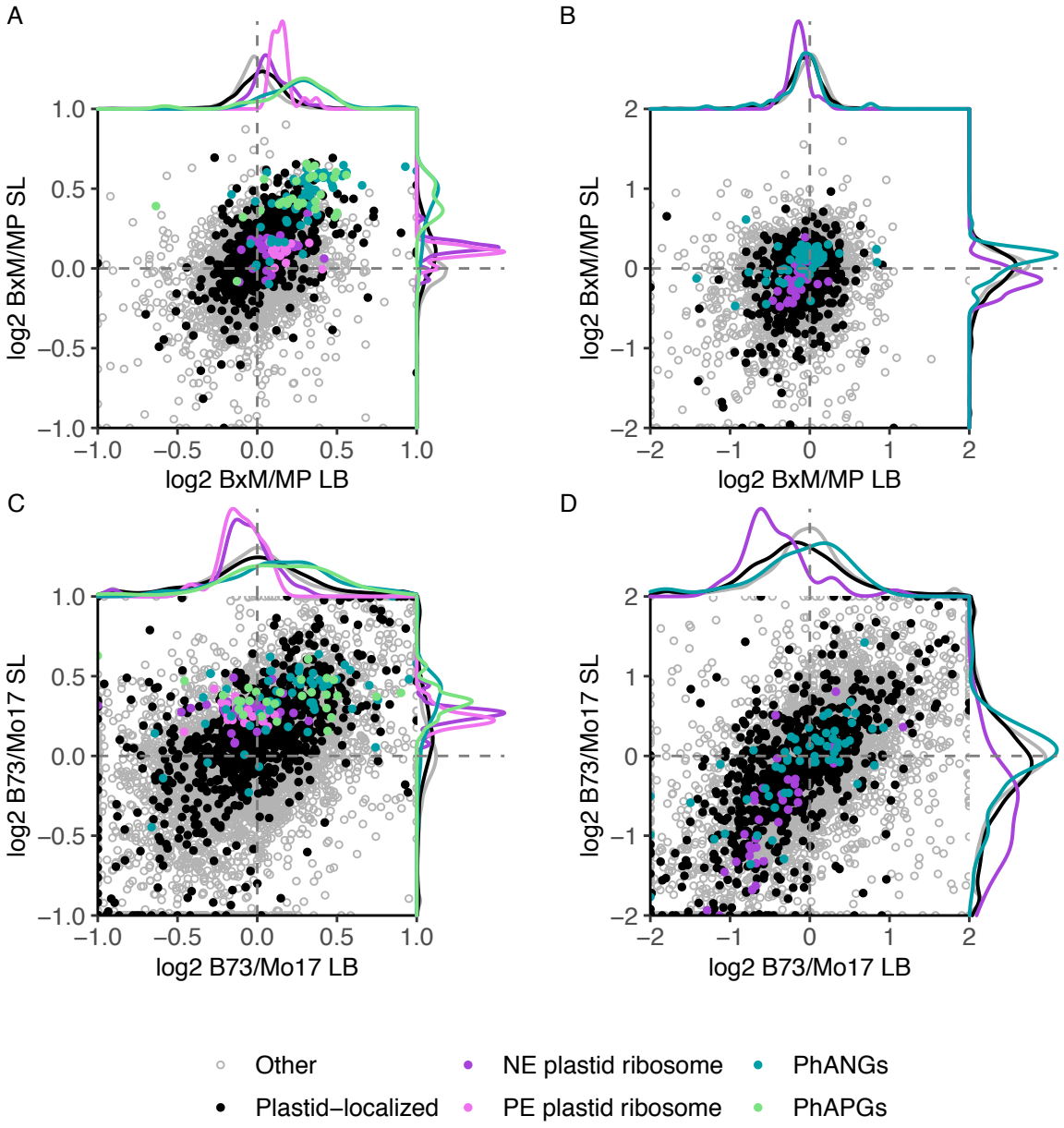

Supplemental Figure 6. Comparison of expression in seedling leaf versus leaf blade tissue. A and B compare hybrid/mid-parent values; C and D compare parent/parent values. A and C show protein; B and D show RNA. Only transcripts for which a protein was detected are shown. Photosynthesis-Associated Nuclear Genes (PhANGs), Photosynthesis-Associated Plastid Genes (PhAPGs), Plastid-Encoded (PE) plastid ribosomes, and Nuclear-Encoded (NE) plastid ribosomes are color-coded.

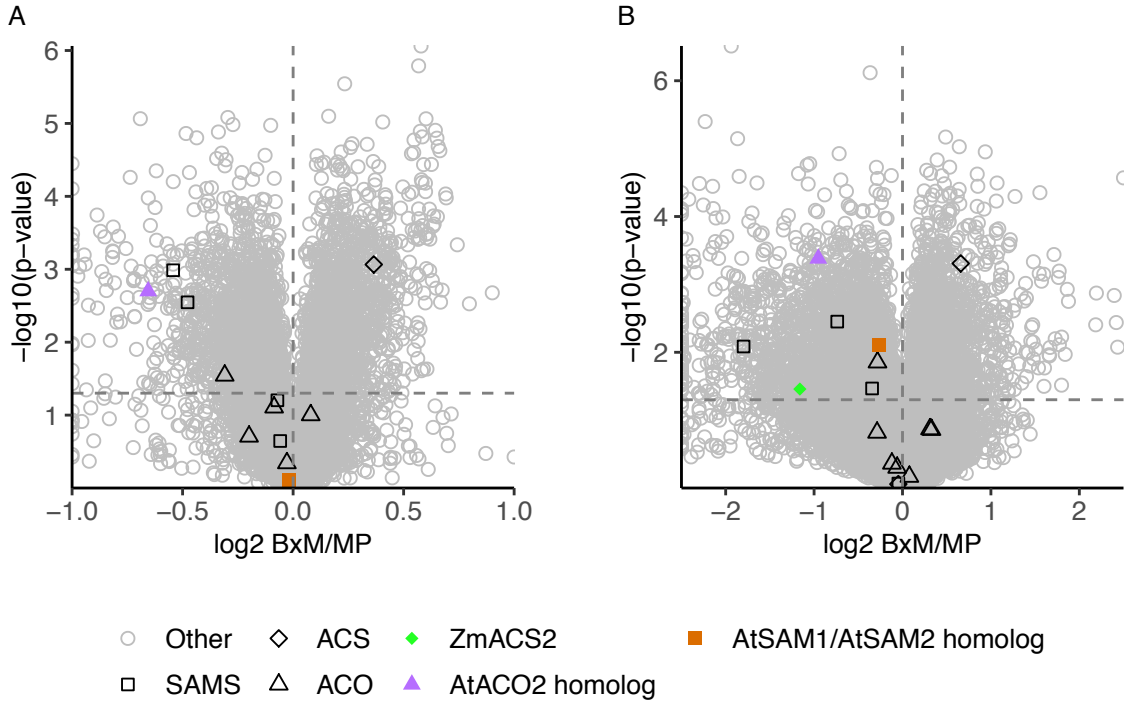

Supplemental Figure 7. Volcano plots showing expression heterosis of ethylene biosynthesis enzymes in the proteome (A) and transcriptome (B) of the BxM hybrid seedling leaf from the original experiment. Of the six enzymes for which the mutant is known to produce reduced ethylene (ZmACS2, ZmACS6, AtACO1, AtACO2, AtSAMS1, and AtSAMS2), two were detected in the proteome (the AtACO2 homolog and the AtSAMS1/AtSAMS2 homolog) and three were detected in the transcriptome (ZmACS2, the AtACO2 homolog and the AtSAMS1/AtSAMS2 homolog).

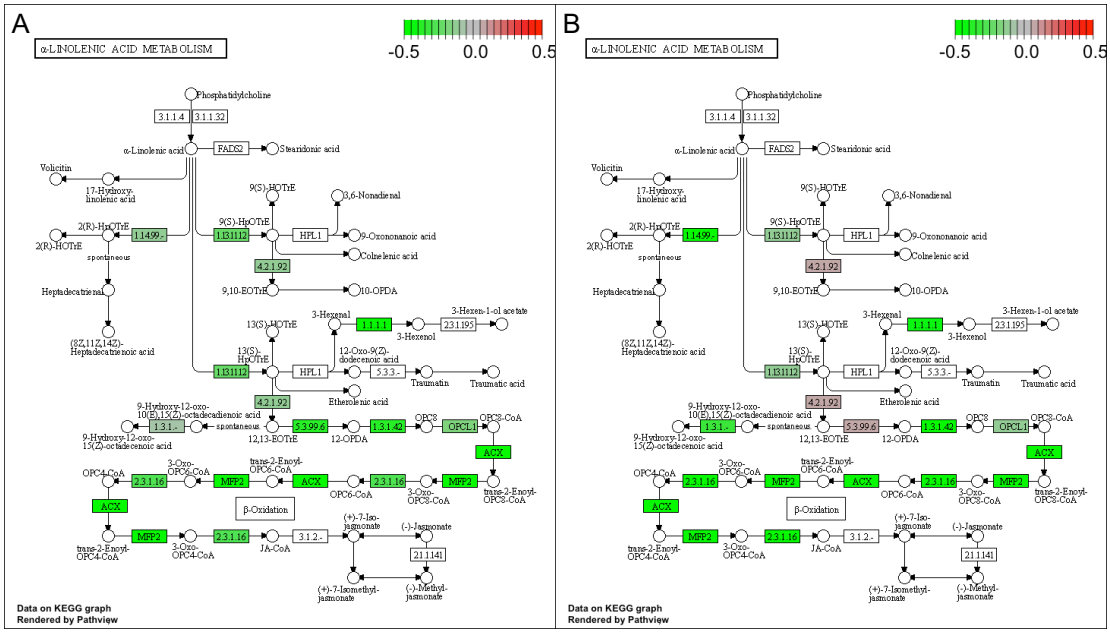

Supplemental Figure 8. Expression of JA biosynthesis enzymes in the (A) hybrid B73xMo17 relative to its mid-parent level; and (B) in the ET biosynthesis mutant (*acs2-6*) relative to its inbred B73 background. Mapped data is provided in Supplemental Figure 5.

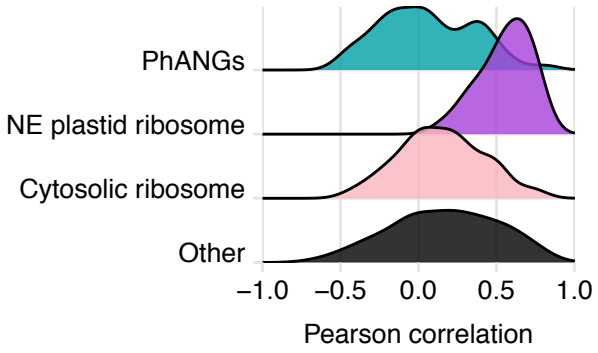

Supplemental Figure 9. Density curves of the Pearson correlations between expression heterosis at the RNA and protein levels in the RIL and six hybrids.

Accession	Pearson	Group
Zm00001d030725_T003	0.95	Plastid
Zm00001d022115_T002	0.92	Other
Zm00001d011993_T002	0.91	NE plastid ribosome
ZemaCp004.1	0.90	PE plastid ribosome
Zm00001d046555_T001	0.90	Plastid
ZemaCp016.1	0.90	PE plastid ribosome
Zm00001d050551_T001	0.89	Other
Zm00001d052075_T001	0.89	Cytosolic ribosome
Zm00001d054107_T002	0.87	Other
Zm00001d027442_T001	0.86	NE plastid ribosome
Zm00001d022421_T001	0.86	Other
Zm00001d012353_T001	0.86	NE plastid ribosome
Zm00001d053713_T001	0.86	Plastid
Zm00001d039613_T002	0.86	Other
Zm00001d052056_T005	0.85	Other
Zm00001d032399_T001	0.85	Other
Zm00001d029201_T001	0.84	NE plastid ribosome
Zm00001d049945_T004	0.84	Other
ZeamMp129.1	0.84	Other
ZemaCp021.1	0.84	PE plastid ribosome
Zm00001d013034_T001	0.84	Cytosolic ribosome
Zm00001d035802_T007	0.84	Other
Zm00001d036565_T001	0.84	Cytosolic ribosome
ZemaCp026.1	0.83	PE plastid ribosome
Zm00001d026690_T001	0.83	Other
Zm00001d015300_T001	0.83	Cytosolic ribosome
ZeamMp081.1	0.83	Other
Zm00001d041036_T001	0.83	Other
Zm00001d044880_T001	0.82	Other
Zm00001d013040_T008	0.82	Other
Zm00001d042454_T001	0.82	Plastid
Zm00001d028240_T001	0.82	NE plastid ribosome
Zm00001d042023_T001	0.82	Other
Zm00001d018412_T001	0.82	NE plastid ribosome
Zm00001d017449_T001	0.81	Plastid
Zm00001d015204_T001	0.81	NE plastid ribosome

ZemaCp058.1	0.81	PE plastid ribosome
Zm00001d047581_T002	0.81	NE plastid ribosome
Zm00001d016276_T001	0.81	Other
Zm00001d043465_T011	0.80	Other
Zm00001d032790_T002	0.80	Other
ZemaCp063.1	0.80	PE plastid ribosome
Zm00001d029968_T001	0.80	Other
ZemaCp062.1	0.80	PE plastid ribosome
Zm00001d022599_T001	0.80	Other
ZemaCp061.1	0.80	PE plastid ribosome
Zm00001d014519_T001	0.80	Other
ZeamMp119.1	0.80	Other
Zm00001d038006_T001	0.80	Other
Zm00001d043170_T001	0.79	Other
ZemaCp046.1	0.79	PE plastid ribosome
Zm00001d038851_T001	0.79	Other
Zm00001d037875_T001	0.79	Other
Zm00001d047462_T001	0.79	NE plastid ribosome

Table 1. The top 1.5% of proteins whose expression heterosis was most correlated with plant height heterosis. Data shown are Pearson correlations.

Experiment	Hybrid	HybridHeight	MomHeight	DadHeight	MPheight	Hyb.MP
RIL	B73xMo17	263.176	226.056	209.556	217.806	1.2083
RIL	M0014xB73	233.000	196.000	226.056	211.028	1.1041
RIL	M0014xMo17	249.000	196.000	209.556	202.778	1.2279
RIL	M0016xB73	257.000	196.000	226.056	211.028	1.2178
RIL	M0016xMo17	230.000	196.000	209.556	202.778	1.1342
RIL	M0021xB73	247.000	205.000	226.056	215.528	1.1460
RIL	M0021xMo17	248.000	205.000	209.556	207.278	1.1965
RIL	M0317xB73	261.000	203.000	226.056	214.528	1.2166
RIL	M0317xMo17	257.000	203.000	209.556	206.278	1.2459
6H	B73xMo17	283.833	218.167	223.667	220.917	1.2848
6H	Mo17xB73	299.500	223.667	218.167	220.917	1.3557
6H	B84xB73	262.333	206.333	218.167	212.250	1.2360
6H	B84xMo17	292.833	206.333	223.667	215.000	1.3620
6H	A682xB73	299.500	208.667	218.167	213.417	1.4034
6H	A682xMo17	254.667	208.667	223.667	216.167	1.1781

Supplemental Table 1. Plant height data for the RIL and six hybrids.

v4_gene_model	Gene.entrez	labels	l2.B73xMo17.MP	l2.ACS.B73
Zm00001d003533	100037808	lox9	NA	-0.10807
Zm00001d009182	100285945	pco097710	-0.08072	-0.18851
Zm00001d014093	100274263	100192501	-0.05863	-0.25662
Zm00001d015852	100037810	lox9	0.02395	-0.30095
Zm00001d015992	100281695	pco097710	-0.17698	-0.08696
Zm00001d018487	100192501	100192501	-0.20519	-0.37331
Zm00001d025166	100216803	100216803	-0.08501	-0.31383
Zm00001d027519	100274307	100274307	-0.16582	-0.11286
Zm00001d027893	100037806	lox9	NA	0.01296
Zm00001d028282	100279433	aos2	0.04716	0.01949
Zm00001d029594	542151	aoc2	-0.22037	-0.04589
Zm00001d033931	542363	adh1	-0.12078	-0.07173
Zm00001d034186	103644066	aos2	NA	-0.09293
Zm00001d035854	101027254	101027254	-0.14887	-0.52191
Zm00001d039768	100283936	100191469	-0.08060	-0.31051
Zm00001d040842	732733	opr3	-0.03428	-0.15435
Zm00001d042884	100285661	100191469	-0.27399	-0.28676
Zm00001d044906	732822	opr3	NA	-0.52939
Zm00001d044908	732815	opr3	-0.17356	-0.19735
Zm00001d045251	100191469	100191469	-0.16323	-0.23883
Zm00001d045606	100382424	100191469	NA	0.22168
Zm00001d047340	100273356	aoc2	-0.14338	0.12102
Zm00001d048021	542150	aos2	-0.18660	0.15961
Zm00001d049059	542364	adh1	-0.58705	-0.32860
Zm00001d050107	732734	opr3	NA	0.09703
Zm00001d053308	103654691	pco097710	-0.31268	-0.37164
Zm00001d053675	100037809	lox9	-0.24191	0.27741

Supplemental Table 2. Expression values of proteins displayed on the KEGG maps in Figure S8.

Experiment	126	127N	127C	128N	128C	129N	129C	130N	130C	131
ACS2_6	B73-r1	B73-r2	B73-r3	B73-r4	B73-r5	acs-r1	acs-r2	acs-r3	acs-r4	acs-r5
Seedling Leaf	Pool	B73-r1	B73-r2	B73-r3	Mo17-r1	Mo17-r2	Mo17-r3	BM-r1	BM-r2	BM-r3
Mature Leaf Blade	Pool	B73-r1	B73-r2	B73-r3	Mo17-r1	Mo17-r2	Mo17-r3	BM-r1	BM-r2	BM-r3
6Hybrid rep1	B73-r1	B84-r1	Mo17-r1	A682-r1	B73xMo17-r1	Mo17xB73-r1	B84xB73-r1	B84xMo17-r1	A682xB73-r1	A682xMo17-r1
6Hybrid rep2	B73-r2	B84-r2	Mo17-r2	A682-r2	B73xMo17-r2	Mo17xB73-r2	B84xB73-r2	B84xMo17-r2	A682xB73-r2	A682xMo17-r2
6Hybrid rep3	B73-r3	B84-r3	Mo17-r3	A682-r3	B73xMo17-r3	Mo17xB73-r3	B84xB73-r3	B84xMo17-r3	A682xB73-r3	A682xMo17-r3
Day	pool	B73-r1	B73-r2	B73-r3	Mo17-r1	Mo17-r2	Mo17-r3	BM-r1	BM-r2	BM-r3
Night	pool	B73-r1	B73-r2	B73-r3	Mo17-r1	Mo17-r2	Mo17-r3	BM-r1	BM-r2	BM-r3
RIL-BxM	B73-r1	B73-r3	B73-r4	Mo17-r1	Mo17-r3	Mo17-r4	BM-r1	BM-r3	BM-r4	BM-r2
RIL14-rep12	B73-r1	B73-r2	Mo17-r1	Mo17-r2	14-r1	14-r2	14B-r1	14B-r2	14M-r1	14M-r2
RIL14-rep34	B73-r3	B73-r4	Mo17-r3	Mo17-r4	14-r3	14-r4	14B-r3	14B-r4	14M-r3	14M-r4
RIL16-rep12	B73-r1	B73-r2	Mo17-r1	Mo17-r2	16-r1	16-r2	16B-r1	16B-r2	16M-r1	16M-r2
RIL16-rep34	B73-r3	B73-r4	Mo17-r3	Mo17-r4	16-r3	16-r4	16B-r3	16B-r4	16M-r3	16M-r4
RIL21-rep12	B73-r1	B73-r2	Mo17-r1	Mo17-r2	21-r1	21-r2	21B-r1	21B-r2	21M-r1	21M-r2
RIL21-rep34	B73-r3	B73-r4	Mo17-r3	Mo17-r4	21-r3	21-r4	21B-r3	21B-r4	21M-r3	21M-r4
RIL317-rep12	B73-r1	B73-r2	Mo17-r1	Mo17-r2	317-r1	317-r2	317B-r1	317B-r2	317M-r1	317M-r2
RIL317-rep34	B73-r3	B73-r4	Mo17-r3	Mo17-r4	317-r3	317-r4	317B-r3	317B-r4	317M-r3	317M-r4

Supplemental Table 3. TMT10 labeling scheme.